PAPER

Design of AlGaN-based lasers with a buried tunnel junction for sub-300 nm emission

IOP ebooks™

Bringing you innovative digital publishing with leading voices to create your essential collection of books in STEM research.

Start exploring the collection - download the first chapter of every title for free.

Design of AlGaN-based lasers with a buried tunnel junction for sub-300 nm emission

Shamsul Arafin[1] [iD]**, Syed M N Hasan[1], Zane Jamal-Eddine[1], Darshana Wickramaratne[2], Banaful Paul[1] and Siddharth Rajan[1]**

[1] Department of Electrical and Computer Engineering, The Ohio State University, Columbus, OH, USA
[2] NRC Research Associate, Resident at Center for Computational Materials Science, US Naval Research Laboratory, Washington, DC, USA

E-mail: arafin.1@osu.edu

CrossMark

Abstract

This paper discusses the design of electrically-pumped AlGaN-based in-plane lasers emitting at $\sim$290 nm. Our laser design utilizes strained $Al_{0.5}Ga_{0.5}N$ quantum wells, and a novel polarization engineered AlGaN/InGaN/AlGaN-based tunnel junction. The low resistive tunnel junction is used as an intracavity contact in the device in place of the resistive p-type contact; which leads to improved hole injection and a reduced threshold voltage. Hence, room-temperature continuous-wave laser operation could be enabled. Strategies to improve the performance of the tunnel junction contact through the incorporation of low concentrations of boron in the highly-doped AlGaN tunnel junction layers as a means to increase the polarization sheet charge are also discussed.

Keywords: molecular beam epitaxy, metalorganic chemical vapor deposition, AlGaN, tunnel junction, UV diode laser

(Some figures may appear in colour only in the online journal)

1. Introduction

Since the first demonstration of the GaN blue laser diode by Nakamura and coworkers in 1996 [1], the performance of laser diodes based on the III-nitride material system continue to improve. This has led to the commercialization of GaN blue laser diodes that are capable of outputting several Watts of power in the wavelength range of 400–500 nm [2]. Despite these excellent demonstrations of aluminium-free nitride-lasers, UV lasers based on AlGaN has still remained a challenge.

Over the last decade or so, a significant amount of research has been devoted towards demonstrating UV-lasers by various research groups [3]. This is mainly because these lasers can enable a number of important and emerging applications including phototherapy in the medical sector [4], water sterilization [5], trace gas sensing [6], polymer curation, indoor plant growth and horticulture, as well as stimulating the formation of anti-cancerogenic substances [7]. Electrically-pumped lasers have been recently achieved down to 336 nm by achieving low defect density templates, and

optimization of materials growth [8, 9]. However, little success has been achieved in shorter wavelength laser diodes for several reasons we outline below.

The principal problems for electrically-pumped AlGaN lasers are related to hole doping, and injection. Light extraction, one of the limiting factors of obtaining high-output power in light-emitting diodes (LEDs), is not an issue in the case of lasers. The combination of extremely high hole ionization energy in AlGaN (400 meV for 70% AlGaN) and high valence band effective mass ($>2m_e$) leads to highly resistive p-AlGaN layers and challenges in making ohmic p-contacts. This makes it very challenging to reach the threshold current densities required for lasing. For example, a current density of $10\,kA\,cm^{-2}$ for a 400 nm pAlGaN layer would require an unrealistic voltage drop of over 200 V [10]. Therefore, an alternate approach such as utilizing buried tunnel junction as an intracavity contact which can reduce electrical losses while maintaining low optical loss is necessary.

The principal advantage of using the tunnel junction over the conventional p-n junction approach includes the ability to
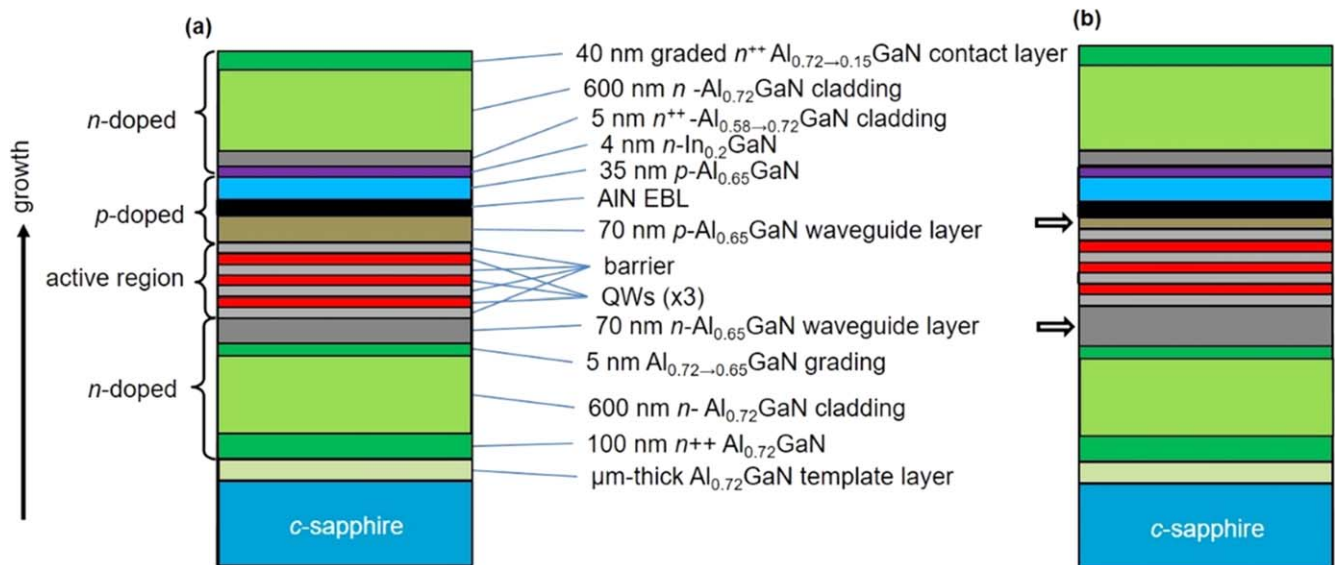
Figure 1. Schematic cross-section of the tunnel junction-based AlGaN laser structure with (a) symmetric and (b) asymmetric configurations, designed for an emission wavelength of 290 nm. The major changes in the asymmetric structure are marked by arrows.

achieve low series resistance, low optical loss and low contact resistance. Since the refractive index contrast available in the III-nitride system is low, thick cladding regions are necessary to achieve good transverse optical confinement. This makes series resistance a major challenge. Using a tunnel junction, both cladding layers can be made *n*-type which provides good optical confinement while still having relatively low contact resistance. In comparison, the *p*-type AlGaN used in the conventional approach would lead to very high resistance. Secondly, due to the use of *n*-doped materials on top of the tunnel junction, intravalence-band absorption can be suppressed. In addition, the tunnel junction can be made very thin using polarization engineering to minimize the optical mode confinement factor in this region, leading to low absorption losses. Thirdly, contact resistance in *n*-AlGaN can be made very low compared to a *p*-AlGaN layer. Furthermore, the conductivity of a tunnel junction increases with current density and applied voltage. Therefore, hole injection through tunneling can become more efficient at the high current densities necessary for a laser.

2. Laser design

The edge-emitting lasers designed in this study are based on a sapphire substrate with a μm-thick metal-polar $Al_{0.7}GaN$ template. The epitaxial structure of the laser structure begins with a 600nm n^+-$Al_{0.65}GaN$ layer for the n-side contact. This layer is followed by a 600 nm n-$Al_{0.65}GaN$ cladding layer, and a quantum well (QW) active region designed for $\lambda = 290$ nm emission. This is followed by a top *p*-waveguide layer and then a 18 nm *p*-AlN electron blocking layer (EBL). The laser structure is completed with p^+-AlGaN/InGaN/n^+-AlGaN tunnel junction layers, 600 nm n^+-$Al_{0.65}GaN$ cladding layer, and a 40 nm reverse compositionally graded heavily-doped *n*-AlGaN with an Al mole

fraction grading from 65% to 15% in order to form the top *p*-side low-resistive ohmic contact. The *p*-AlN EBL is deliberately placed right above the QWs to improve hole injection. Otherwise, the valence band barrier or positive polarization at the bottom AlN/waveguide interface will jeopardize hole injection into the active region.

The two laser structures designed in this study are expected to enable sufficient carrier injection with a reasonable voltage drop to achieve electrically-pumped lasing. The symmetric FP structure where the QWs are centered with respect to the waveguide are presented in figure 1(a). With this design, the tunnel junction is located just only 100 nm away from the peak of the optical mode. This design leads to a strong overlap of this mode with the highly absorbing tunnel junction. In an ideal case, such a mode should have a node at the position of the tunnel junction to reduce free carrier absorption loss. Therefore, we refined our laser design by deliberately placing the QWs on top of the bottom *n*-doped waveguide, as shown in figure 1(b). In this configuration, the optical mode overlap with the multi-quantum wells (MQWs) is not the maximum possible level since they are not at the center of the top and bottom waveguide layers. However, the mode overlap with the tunnel junction is reduced since it is farther away from the active region. Hence, this asymmetric design greatly minimizes the optical loss and simplifies the laser structure by retaining the FP configuration.

2.1. Materials growth technology selection

The tunnel-injected deep-UV structure will be grown on a metal-polar $Al_{0.72}Ga_{0.28}N$/c-plane sapphire template. Both metalorganic chemical vapor deposition (MOCVD) and molecular beam epitaxy (MBE) growth technologies can be used to grow such a structure. Due to the use of the non-conductive substrate, the growth will be initiated by the highly doped *n*-contact layer. A base structure containing the template, *n*-contact layer, lower cladding, the optical

waveguide and the MQW active region, is first grown using MOCVD. A second 'regrowth' will then be performed using MBE to grow the tunnel junction, top cladding and the top *p*-side contact. Compressively-strained QWs are used in this design to reduce the difference in effective masses between holes and electrons, and thus the difference in density of states in the valence and conduction bands. This enables more gain for a given input current as well as a higher differential gain, both key desirable features of laser gain material. It has already been demonstrated that MOCVD-grown active region exhibits much better optical performance compared to MBE grown active regions. In contrast, MOCVD-grown tunnel junction is found to be highly-resistive due to poor doping of the tunnel junction layers. Furthermore, one achieves relatively sharper interfaces in MBE-grown ultra-thin layers, requiring twofold epitaxial growth in getting functional devices.

2.2. Active region and tunnel junction

The active region used in this device consists of three compressively strained 2-nm-thick $Al_{0.5}Ga_{0.5}N$ QWs separated by 6 nm $Al_{0.65}Ga_{0.35}N$ barriers. In case of the symmetric structure, the outer parts of the QWs are surrounded by 70nm thick doped $Al_{0.65}Ga_{0.35}N$ separate confinement layers. The band diagram of the active region is presented in figure 2(a). Details of this active region to obtain LEDs emitting at 287 nm with 2.8% external quantum efficiency can be found elsewhere [11].

The tunnel junction layer consists of p^+-AlGaN with Mg doping concentration of $5 \times 10^{19}\,cm^{-3}$, 4 nm $In_{0.2}Ga_{0.8}N$, and 5 nm n^+-AlGaN with Si doping concentration of $10^{20}\,cm^{-3}$ with the Al composition grading from 58% to 65%. The simulated energy band diagram, as shown in figure 2(b) confirms a sharp band alignment obtained through such a tunnel junction design. Details of this low-resistive and nearly ohmic tunnel junction can be found elsewhere [12].

Since the expected threshold current for AlGaN based lasers could be high, it is critical to ensure that the series resistance of the device is low. This is the most important advantage of tunnel junctions for electrically injected lasers. Based on previous reports of tunnel junction performance, we can achieve a series resistance lower than 1 mΩ-cm^2 for 75% AlGaN. This corresponds to a resistive voltage drop of less than 5 V at a current density of 5 kA cm^{-2}. In comparison, if a *p*-layer was used as the top cladding layer, we can estimate that the series resistance of the stack would exceed 40 mΩ-cm^2, leading to a voltage drop >100 V for 5 kA cm^{-2}.

2.3. Simulated optical characteristics

The laser is designed so that the optical mode overlap with the MQWs is at the maximum possible level. By definition, the modal gain also is the maximum achievable. As a standard practice, one improves the optical mode overlap with QWs as much as possible while obtaining the reduced mode overlap with the substrate and highly doped contact and tunnel junction layer at the same time. Figure 3 shows the 1D and
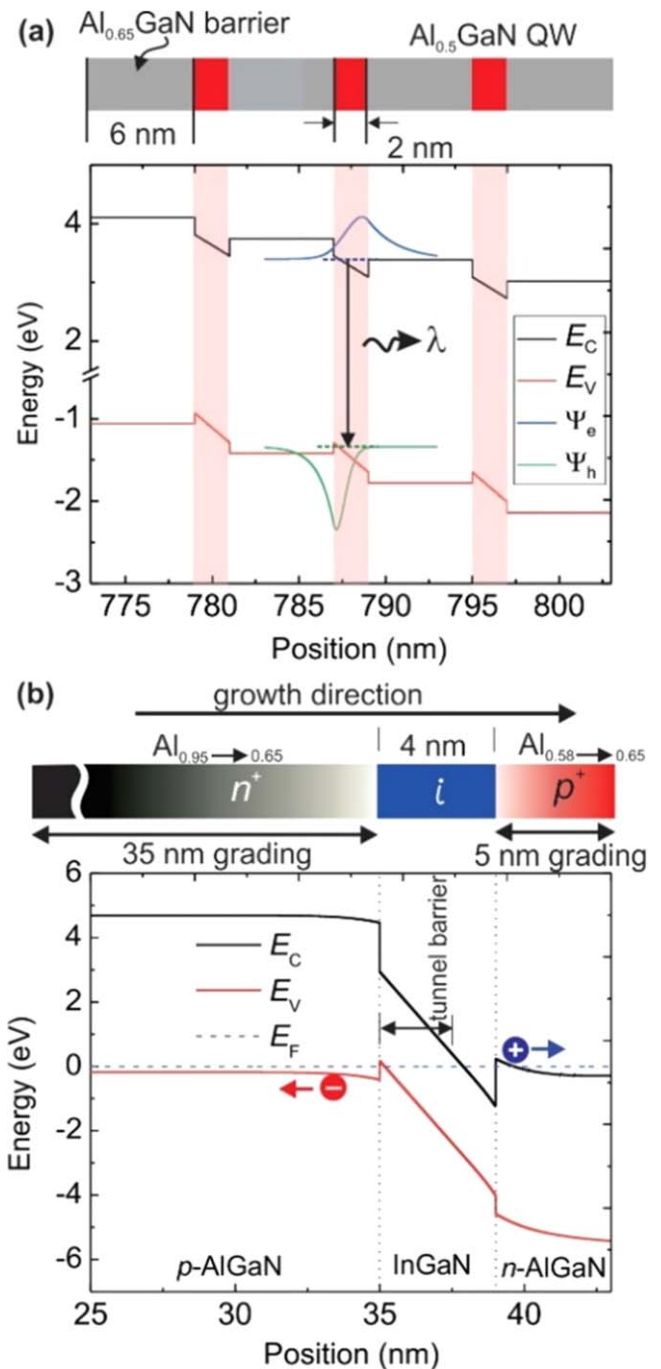

Figure 2. Simulated equilibrium energy band diagram of the (a) active region and (b) tunnel junction that is used in the UV-B laser designed at ~290 nm.

2D intensity distribution of the fundamental transverse mode in the ~290 nm laser structure. The intensity distribution together with the refractive index profile is also shown here.

The optical confinement factor Γ of a semiconductor laser is of utmost importance. Considering the material gain curve is constant, increasing the optical confinement factor yields an increase in the modal gain. Figure 3(d) lists the values for Γ in several regions of the laser waveguide by which our design can be assessed. In case of an asymmetric design, as presented in figure 4, the mode overlap with the
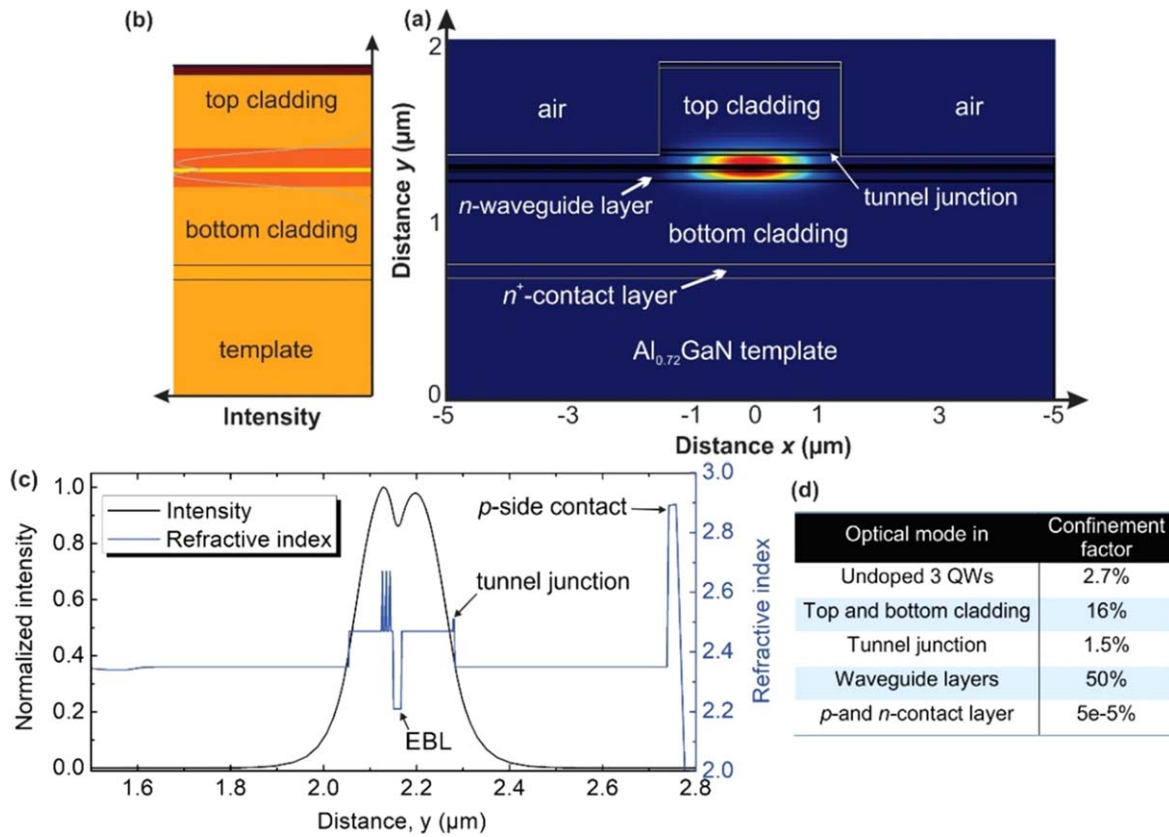
Figure 3. (a) Cross section of a 290 nm symmetric laser structure along with a 2D surface plot of the light intensity of the fundamental transverse mode, where the waveguide effective refractive index $n_{\text{eff}} = 2.42$, (b) 1D intensity distribution of the fundamental TE-mode in the waveguide, (c) refractive index profile and mode intensity distribution, and (d) confinement factors in several sections of the laser structure.

tunnel junction is reduced by more than a factor of 7 without sacrificing Γ for the active region significantly. Figure 4(d) lists the Γ values in several regions of the asymmetric laser resonator.

It should be noted that the undoped InGaN layer which is as thin as 4 nm located at the center of the tunnel junction in our laser structure will be mainly responsible for the optical absorption since the top and bottom heavily-doped p- and n-grading layers should be depleted of carriers, resulting in minimal absorption loss. Another consideration in this design should be made by the following absorption coefficient which is given as [13]

$$\alpha_{\text{FC}} = \frac{e^3 \lambda^2}{4\pi^2 c^3 \varepsilon_0 n} \left(\frac{N}{m_e^{*2} \mu_e} + \frac{P}{m_h^{*2} \mu_h} \right)$$

where c is the speed of light, $\in_0$ the dielectric constant, N and P the electron and hole densities, respectively, and m_e, m_h, μ_e, μ_h are the electron and hole effective masses and mobilities, respectively. Thus, the absorption by free carriers gets weaker, the shorter the wavelength. Due to the dependence on λ^2, this loss mechanism will not be that prominent in the ultra-short wavelength devices.

Unlike the other III–V compound semiconductor-based lasers, III-nitride surfaces provide a reflectivity of only ~19% from the naturally-cleaved facet at the semiconductor-air interface. This may necessitate a high-reflection (HR) coating on one of the facets in order to overcome the resonator losses.

A metal–dielectric mirror is proven to be a simple solution for high-reflectivity coatings on cleaved-facet edge-emitting lasers. A simple Al_2O_3/Al coating with a reflectivity of more than 95% could be used. To circumvent the potential reduction in reflectivity due to the facile oxidation of Al we also propose the use of multi-layer stacked SiO_2/HfO_2 layers for HR coating as an alternative.

3. Polarization engineering with boron alloys

We also consider strategies to enhance our proposed design of the AlGaN/InGaN/AlGaN tunnel junction. Boron containing III-nitride alloys are recently being explored for ultraviolet optoelectronics. Alloying the III-nitrides with boron expands the design space across which polarization charges and band gaps can be accessed. While BN is stable in the hexagonal phase, there have been several experimental demonstrations of stable wurtzite BAlN and BGaN alloys [14, 15]. First-principles calculations have shown the fundamental band gap of wurtzite BN (wz-BN) is 6.84 eV and that wz-BN also exhibits the largest spontaneous polarization of the conventional III-nitrides [16]. Incorporating a fraction of boron into the n^{++} and p^{++} AlGaN regions of the tunnel junction could lead to enhanced polarization charges at the $B_y Al_x Ga_{(1-y-x)} N / In_{0.2} Ga_{0.8} N$ interface compared to an $Al_x Ga_{(1-x)} N / In_{0.2} Ga_{0.8} N$ interface. Larger bound charges at
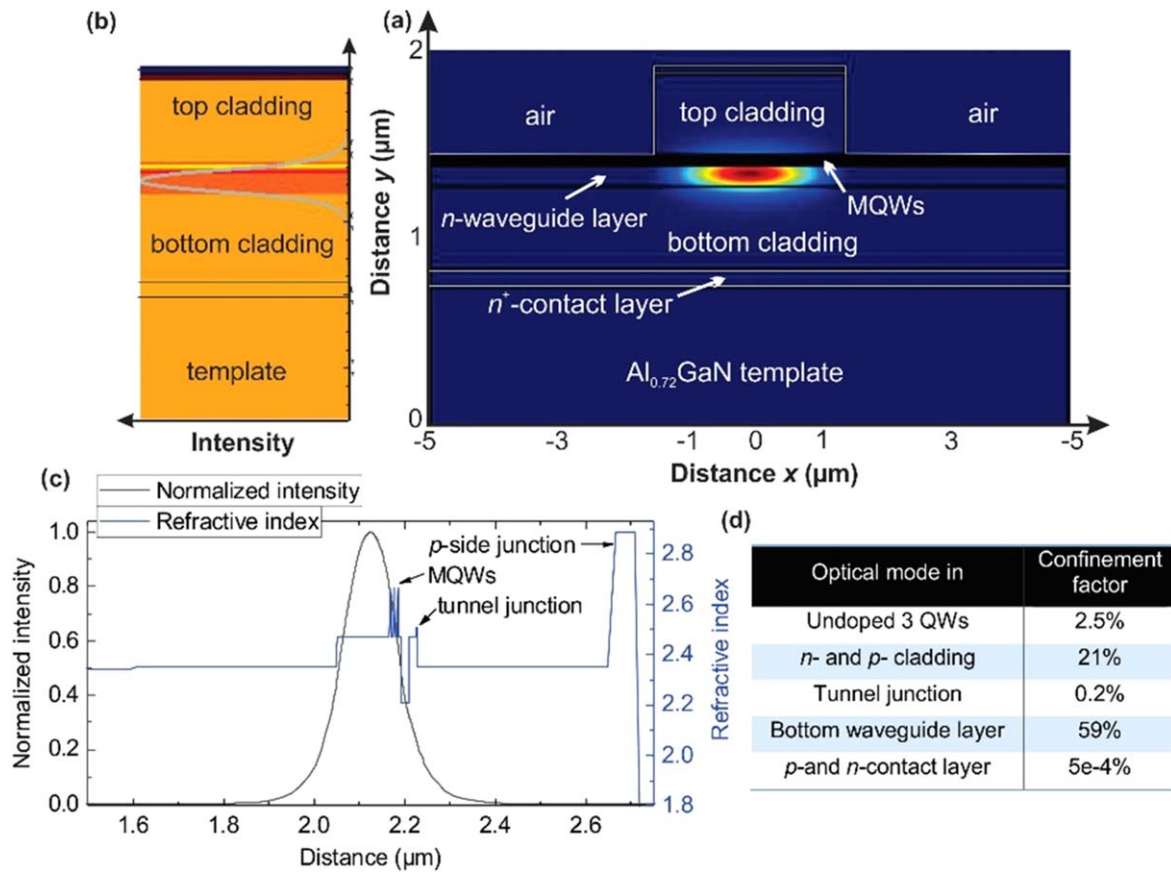
Figure 4. (a) Cross section of a 290 nm symmetric laser structure along with a 2D surface plot of the light intesnity of the fundamental transverse mode, where the waveguide effective refractive index $n_{eff} = 2.42$, (b) 1D intensity distribution of the fundamental TE-mode in the waveguide, (c) refractive index profile and mode intensity distribution, and (d) confinement factors in several sections of the offset-QW-based laser structure.

the interface would decrease the tunneling distance across the junction [17] and decrease the resistance across the tunnel junction. To this end we calculate the magnitude of the bound charge at an AlGaN/In$_{0.2}$Ga$_{0.8}$N interface as a function of Alcontent and a B$_y$Al$_x$Ga$_{(1-y-x)}$N/In$_{0.2}$Ga$_{0.8}$N interface as a function of Al content for 1% and 4% boron. We use the spontaneous and piezoelectric polarization constants for the III-nitrides obtained from first principles [16, 18] and elastic constants reported in [19]. The spontaneous and piezoelectric polarization constants, lattice constants and elastic tensors are assumed to vary linearly with alloy content. These results are illustrated in figure 5. It is evident that for all concentrations of Al, the B containing BAlGaN alloys lead to a larger bound charge at the BAlGaN/InGaN interface compared to the AlGaN/InGaN interface. Hence, we suggest the incorporation of B in the AlGaN regions of the tunnel junction can be used to obtain larger bound charges and in turn a lower tunnel junction resistance in UV optoelectronics.

4. Conclusion

In summary, we have presented comprehensive design details of electrically-pumped AlGaN-based UV-B laser diodes that can provide lower threshold voltage and continuous-wave
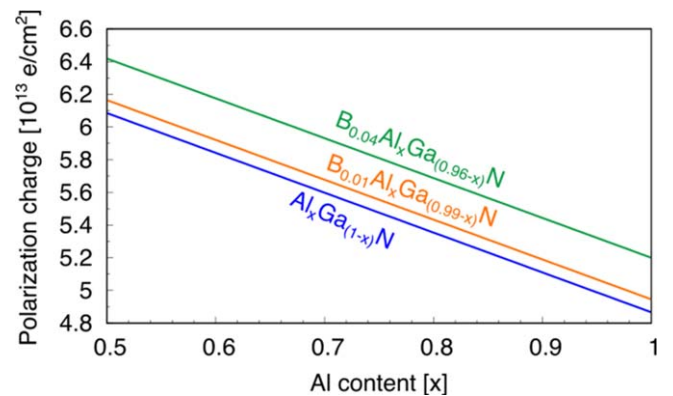

Figure 5. Polarization charge at interfaces between Al$_x$Ga$_{(1-x)}$N/In$_{0.2}$GaN (blue), B$_{0.01}$Al$_x$GaN$_{(0.99-x)}$/In$_{0.2}$Ga$_{0.8}$N (orange) and B$_{0.04}$Al$_x$GaN$_{(0.96-x)}$/In$_{0.2}$Ga$_{0.8}$N (green) as a function of Al content.

operation. The design utilizes interband tunneling to replace the highly-resistive *p*-doped layers on top of the active region by an *n*-doped region. Our calculations also show we expect device performance to improve further with the use of boron-containing AlGaN layers in the tunnel junctions. In our future efforts, we will grow *wz*-BAlN layers with controlled boron content by MBE to achieve its full potential. After optimizing the materials growth and finding the reasonable interface or

surface roughness of these layers, we will then fabricate such boron-containing tunnel juxtion test structures to explore our theoretical designs proposed here.

Acknowledgments

ORCID iDs

Shamsul Arafin ⬤ https://orcid.org/0000-0003-4689-2625

References

[1] Nakamura S, Senoh M, Nagahama S I, Iwasa N, Yamada T, Matsushita T, Sugimoto Y and Kiyoku H 1996 Room-temperature continuous-wave operation of InGaN multi-quantum-well structure laser diodes *Appl. Phys. Lett.* **69** 4056

[2] Brüninghoff S, Eichler C, Tautz S, Lell A, Sabathil M, Lutgen S and Strauß U 2009 8 W single-emitter InGaN laser in pulsed operation *Phys. Stat. Sol.* (a) **206** 1149

[3] Kuhn C *et al* Influence of waveguide strain and surface morphology on AlGaN-based deep UV laser characteristics 2018 *J. Phys. D: Appl. Phys.* **51** 415101

[4] Honigsmann H 2013 History of phototherapy in dermatology *Photochem. Photobiol. Sci.* **12** 16

[5] Lange M A, Kolbe T and Jekel M 2016 Ultraviolet light-emitting diodes for water disinfection *III-Nitride Ultraviolet Emitters : Technology and Applications* (Switzerland: Springer) 2016

[6] Albrecht C and Lakowicz J R 2008 Principles of fluorescence spectroscopy 3rd edition *Anal. Bioanal. Chem.* **390** 1223

[7] Neugart S, Zietz M, Schreiner M, Rohn S, Kroh L W and Krumbein A 2012 Structurally different flavonol glycosides and hydroxycinnamic acid derivatives respond differently to moderate UV-B radiation exposure *Physiol Plant* **145** 582

[8] Yoshida H, Yamashita Y, Kuwabara M and Kan H 2008 Demonstration of an ultraviolet 336 nm AlGaN multiple-quantum-well laser diode *Appl. Phys. Lett.* **93** 241106

[9] Kneissl M, Yang Z, Teepe M, Knollenberg C, Schmidt O, Kiesel P, Johnson N M, Schujman S and Schowalter L J 2007 Ultraviolet semiconductor laser diodes on bulk AlN *J. Appl. Phys.* **101** 123103

[10] Nakarmi M L, Kim K H, Khizar M, Fan Z Y, Lin J Y and Jiang H X 2005 Electrical and optical properties of Mg-doped $Al_{0.7}Ga_{0.3}N$ alloys *Appl. Phys. Lett.* **86** 092108

[11] Zhang Y *et al* Tunnel-injected sub 290 nm ultra-violet light emitting diodes with 2.8% external quantum efficiency 2018 *Appl. Phys. Lett.* **112** 071107

[12] Zhang Y, Krishnamoorthy S, Akyol F, Allerman A A, Moseley M W, Armstrong A M and Rajan S 2016 Design and demonstration of ultra-wide bandgap AlGaN tunnel junctions *Appl. Phys. Lett.* **109** 121102

[13] Buus J, Amann M-C and Blumenthal D J 2005 *Tunable Laser Diodes and Related Optical Sources* (Piscataway, NJ: Wiley-IEEE Press)

[14] Li X, Wang S, Liu H, Ponce F A, Detchprohm T and Dupuis R D 2017 100-nm thick single-phase wurtzite BAlN films with boron contents over 10% *Phys. Stat. Sol.* (b) **254** 1600699

[15] Malinauskas T, Kadys A, Stanionytė S, Badokas K, Mickevičius J, Jurkevičius J, Dobrovolskas D and Tamulaitis G 2015 Growth of BGaN epitaxial layers using close-coupled showerhead MOCVD *Phys. Stat. Sol.* (b) **252** 1138

[16] Dreyer C E, Lyons J L, Janotti A and Van 2014 de Walle C G 'Band alignments and polarization properties of BN polymorphs *Appl. Phys. Express* **7** 031001

[17] Krishnamoorthy S, Nath D N, Akyol F, Park P S, Esposto M and Rajan S 2010 Polarization-engineered GaN/InGaN/GaN tunnel diodes *Appl. Phys. Lett.* **97** 203502

[18] Dreyer C E, Janotti A, Van de Walle C G and Vanderbilt D 2016 Correct implementation of polarization constants in wurtzite materials and impact on III-nitrides *Phys. Rev. X* **6** 021038

[19] Vurgaftman I and Meyer J R 2003 Band parameters for nitrogen-containing semiconductors *J. Appl. Phys.* **94** 3675